A Quantum Wave Packet Dynamics Study of the N(^{2}D) + H_2 Reaction†

Tian-Shu Chu,‡ Ke-Li Han,‡ and António J. C. Varandas*,§

State Key Laboratory of Molecular Reaction Dynamics, Dalian Institute of Chemical Physics, Chinese Academy of Sciences, Dalian 116023, China, and Departamento de Química, Universidade de Coimbra, 3004-535 Coimbra, Portugal

Received: August 15, 2005; In Final Form: October 24, 2005

We report a dynamics study of the reaction N(^{2}D) + H_2 (v=0, j=0−5) → NH + H using the time-dependent quantum wave packet method and a recently reported single-sheeted double many-body expansion potential energy surface for NH_2(1^2A″) which has been modeled from accurate ab initio multireference configuration-interaction calculations. The calculated probabilities for (v=0, j=0−5) are shown to display resonance structures, a feature also visible to some extent in the calculated total cross sections for (v=0, j=0). A comparison between the calculated centrifugal-sudden and coupled-channel reaction probabilities validate the former approximation for the title system. Rate constants calculated using a uniform J-shifting scheme and averaged over a Boltzmann distribution of rotational states are shown to be in good agreement with the available experimental values. Comparisons with other theoretical results are also made.

1. Introduction

Compared with the case of ground-state atomic nitrogen, N(^{4}S), the reaction of N(^{2}D) with molecular hydrogen is significantly more reactive and hence accessible to experimental measurement. Although evidence of an abstraction mechanism for this reaction has been reported in an early experimental work[1] on the vibrational distribution of the NH product as well as in several calculations,[2,3] it is now widely recognized that such a reaction belongs to the family of insertion reactions occurring on potential energy surfaces with deep wells. For this reason, experimental and theoretical work[4−15] has recently been diverted to it from the prototype O(^{1}D) + H_2 reaction which has been the most extensively studied thus far.[16−19]

The first global potential energy surface for the 1 ^{2}A″ state of NH_2 favoring an insertion mechanism for the title reaction has been reported by Pederson et al.[4] using the reproducing kernel Hilbert space (RKHS) interpolation method based on high level ab initio points. Using this surface, the same group performed detailed quasiclassical trajectory (QCT) studies[4,10] of the title reaction, having found that the calculated forward−backward symmetric angular distribution and vibrational distributions in the products were in good agreement with the experimental measurements of Umemoto et al.[5,6] This ab initio surface has also been utilized for quantum mechanical studies[7−9] of the title reaction with good results. In particular, time-independent quantum studies[7] led to differential cross sections characteristic of a forward−backward symmetry, in good agreement with the available measurements.[6] Such an observation is indicative of insertion dynamics, thus disputing earlier experimental results[1] that suggested a population inversion in the product nascent vibrational distribution. Further confirmation comes from a combined experimental plus theoretical investigation by Balucani et al.,[8] who have found good agreement between the calculated quantum time-independent and experimental differential cross sections. This group[8] has also discussed quantum effects in the title reaction by comparing their results with those obtained from QCT calculations. In turn, Alagia et al.[9] extended such studies to the N(^{2}D) + D_2 reaction having found that both the experimental and QCT results show nearly backward-forward symmetric product angular distributions. Since there are five electronic doublet states correlating with the N(^{2}D) + H_2 reactants, the title reaction can also serve as a prototype for studying nonadiabatic effects, an issue recently addressed by Schatz and co-workers[10,11] who have performed QCT calculations using the two surfaces of ^{2}A″ and ^{2}A′ symmetries that form a Renner-Teller coupled pair of $^2\Pi$ symmetry. Although the ^{2}A′ state correlates adiabatically with the $a^1\Delta$ state of NH, rather than with the $^3\Sigma^-$ state of interest in the present work, it may still contribute to production of NH($^3\Sigma^-$) + H due to the Renner-Teller degeneracy with ^{2}A″ (the locus of degeneracy corresponds to a one-dimensional seam in the three-dimensional configuration space of the molecule) for linear HNH geometries.

Further theoretical efforts focusing on the refinement and improvement of the 1^2A″ potential energy surface of NH_2 should also be mentioned at this stage, in particular the work of Ho et al.,[12] Varandas and Poveda,[20] and Qu et al.[13] The former group reported a new RKHS potential energy surface for the 1 ^{2}A″ state of NH_2 based on 2715 multireference configuration-interaction (MRCI) points of similar quality as those reported in their earlier study,[4] while the other two groups have almost simultaneously calculated potential energy surfaces for the same system from internally contracted MRCI calculations using an aug-cc-pVQZ basis set. By interpolating their MRCI points with three-dimensional cubic splines and using an additional potential energy surface for the lowest quartet surface of NH_2, Qu et al.[13] have further run QCT calculations of the rate constant for the reactions NH + D → ND + H and NH + D → N + HD and compared the results with their own experimental measurements.

In turn, Varandas and Poveda[20] modeled an accurate DMBE (double many-body expansion) potential energy surface for NH_2-(1 ^{2}A″) by using their own 1498 MRCI/aug-cc-pVQZ points

† Part of the special issue "William Hase Festschrift".

* Corresponding author e-mail address: varandas@qtvs1.qui.uc.pt.
‡ Chinese Academy of Sciences.
§ Universidade de Coimbra.

10.1021/jp054572n CCC: $33.50
Published on Web 12/06/2005

(as well as the MRCI/aug-cc-pV5Z ones, both suitably extrapolated to the complete basis set/infinite CI expansion limits via the DMBE-SEC[21] method, where SEC stands for scaling of the external or dynamical correlation) in the calibration procedure. They have also employed[20] a novel switching function to approximately account for the multisheeted nature of the $NH_2(1\ ^2A'')$ potential energy surface at the dissociation limits. It should be emphasized that the MRCI/aug-cc-pV5Z points played a key role in improving the description of the DMBE potential energy surface at the N−H_2 van der Waals minimum. Indeed, the MRCI/aug-cc-pVTZ calculations (and hence the RKHS[4,12] potential energy surfaces) predict a single C_{2v} van der Waals minimum, while higher-level ab initio MRCI calculations employing aug-cc-pVQZ and aug-cc-pV5Z basis sets show C_{2v} and $D_{\infty h}$ minima connected via a C_s transition state. Since the root-mean-square-deviation achieved on the DMBE calibration procedure is likely to fall within the accuracy of the corrected ab initio points, there are good reasons to believe that it possibly provides the most accurate global form thus far reported to describe both the spectroscopy and reaction dynamics of NH_2 ($1^2A''$). This issue will be further addressed below when discussing the dynamics results obtained for the title reaction on the DMBE[20] potential energy surface by using the time-dependent quantum wave packet method.

Specifically, we report probabilities, total cross sections, and rate constants for the title reaction, with various rotational states of the reactant H_2 being considered. Furthermore, we examine the influence of the Coriolis coupling by performing a limited number of accurate quantum calculations for the title reaction. For each of the selected initial rotational states (j=1−5), the calculations have been carried out at several values of the total angular momentum quantum number J, and these results suitably extrapolated through the popular J-shifting scheme to obtain rate constants. A comparison of these rate constants with available experimental measurements is then also presented. It should be mentioned that no state-to-state attributes will be here reported as the employed computational methodology is unsuitable for such an analysis. Thus, vibrational and rotational distributions of the product NH will be lacking, although this should not affect our fundamental understanding of the title reaction.

The paper is organized as follows. Section 2 surveys the quantum dynamical method, while the results and discussion are presented in section 3. The conclusions are in section 4.

2. Method

The pivotal idea in the quantum wave packet method[22,23] is the use of the split-operator propagation scheme[24] to numerically solve the time-dependent nuclear Schrödinger equation. Two features, namely the fast Fourier transform (FFT)[25] and discrete variable representation (DVR)[26] methods, make it a very efficient tool in studying elementary chemical reactions. For a triatomic system such as NH_2, the Hamiltonian expressed in terms of the reactants' Jacobi coordinates assumes the form

$$H = -\frac{\hbar^2}{2\mu_R}\frac{\partial^2}{\partial R^2} + \frac{(\hat{J}-\hat{j})^2}{2\mu_R R^2} + \frac{\hat{j}^2}{2\mu_r r^2} + V(\vec{R},\vec{r}) + h(r) \quad (2.1)$$

where R is the distance from the N atom and the center-of-mass of H_2, r is the vibrational coordinate of the diatomic, μ_R is the reduced mass of N and H_2, μ_r is the reduced mass of H_2, and $J(j)$ is the total angular momentum (rotational angular momentum quantum number of H_2). In turn, $h(r)$ is the reference Hamiltonian defined by

$$h(r) = -\frac{\hbar^2}{2\mu_r}\frac{\partial^2}{\partial r^2} + V(r) \quad (2.2)$$

with $V(r)$ being the diatomic potential function. Note that $V(\hat{R},\hat{r})$ is the DMBE interaction potential energy surface for the $1\ ^2A''$ state of NH_2.

The following split-operator scheme[24] is used to propagate the initial wave packet on the potential energy surface

$$\psi^{JM\epsilon}(\vec{R},\vec{r},t+\Delta) = e^{-iH_0\Delta/2}e^{-iU\Delta}e^{-iH_0\Delta}/2\psi(\vec{R},\vec{r},t) \quad (2.3)$$

where H_0 is the reference Hamiltonian, and U is the effective potential:

$$H_0 = -\frac{\hbar^2}{2\mu_R}\frac{\partial^2}{\partial R^2} + h(r) \quad (2.4)$$

$$U = \frac{(\hat{J}-\hat{j})^2}{2\mu_R R^2} + \frac{\hat{j}^2}{2\mu_r r^2} + V(\hat{R},\hat{r}) \quad (2.5)$$

In turn, ψ is the wave packet which is here expanded in terms of the body-fixed (BF) translational−vibrational−rotational basis[23] $\{u_n^v(R)\phi_v(r)Y_{jK}^{JM\epsilon}(\hat{R},\hat{r})\}$, where n and v are indices (quantum numbers) labeling the translational and vibrational eigenfunctions, and M and K are the projection quantum numbers of the total angular momentum J on the space-fixed z axis and BF z axis, respectively, and ϵ is the parity of the system. To get converged results in the wave packet expansion, we have used 250 translational basis functions covering the range $0 \le R/a_0 \le 19$ (145 translational basis functions in the interaction region), 111 vibrational basis functions covering the range $0.5 \le r/a_0 \le 15.0$, and rotational basis functions up to $j_{max} = 95$. Moreover, a limit of 40 000 au (960 fs) has been set for the propagation time. All calculations have been done using the centrifugal sudden (CS) approximation. In addition, a limited number of coupled-channel (CC) calculations has been carried out for $J = 10$ and 15 to assess the influence of neglecting the Coriolis coupling in the CS approximation, with the number of K states used in the CC calculations being equal to 5.

The reaction probability can be extracted by calculating the flux at a fixed surface of the corresponding time-independent part of the wave function, $\psi(E)$, after propagation for a sufficient long time[23]

$$P^J_{v_0 j_0 k_0}(E) = \frac{\hbar}{\mu_r}\mathrm{Im}[\langle\psi(E)|\delta(r-r_0)|\psi(E)\rangle] \quad (2.6)$$

where v_0, j_0, and k_0 (the projection quantum number of j_0) are the initial quantum numbers to denote the initial rovibrational state, and $r_0 = 11a_0$ the position where the flux analysis is carried out. The total reaction cross section is then obtained from

$$\sigma_{v_0 j_0 k_0}(E) = \frac{\pi}{k^2}\sum_J (2J+1)P^J_{v_0 j_0 k_0}(E) \quad (2.7)$$

$$\sigma_{v_0 j_0}(E) = \frac{1}{2j_0+1}\sum_{k_0}\sigma_{v_0 j_0 k_0}(E) \quad (2.8)$$

where k is the wavenumber corresponding to the initial state at a fixed collision energy E, and the summations in eqs 2.7 and

2.8 extend to all possible values of J and k_0, respectively. Finally, the rate constant is calculated from the total reaction cross section for a given initial rovibrational state of H_2 by using the expression[27]

$$k_{v_0j_0}(T) = \sqrt{\frac{8k_BT}{\pi\mu_R}}(k_BT)^{-2}\int_0^\infty E\sigma_{v_0j_0}(E)\exp\left(-\frac{E}{k_BT}\right)dE \quad (2.9)$$

where k_B is the Boltzmann constant. The J-shifting method[28,29] has been employed to model the dependence of the reaction probability on J, being calibrated for all studied j states from the calculations explicitly carried out for a few specific J values. It leads to

$$k_{v_0j_0}(T) = \sqrt{\frac{2\pi}{(\mu k_BT)^3}}Q^0_{v_0j_0}(T)\sum_J(2J+1)e^{-B_J(T)J(J+1)/k_BT} \quad (2.10)$$

where the J-shifting constant is defined by[29]

$$B_J(T) = \frac{k_BT}{J(J+1)}\ln\left(\frac{Q^0_{v_0j_0}}{Q^J_{v_0j_0}}\right) \quad (2.11)$$

and Q^0_{v0j0} and Q^J_{v0j0} are partition-like functions defined by

$$Q^0_{v_0j_0} = \int P^0_{v_0j_0}(E)e^{-E/k_BT}dE$$

$$Q^J_{v_0j_0} = \int P^J_{v_0j_0}(E)e^{-E/k_BT}dE \quad (2.12)$$

where the numerical integrations extend to all contributed collision energies, $0.01 \le E/E_h \le 1.0$.

Finally, rotationally averaged rate constants can be obtained by averaging over a Boltzmann distribution of such states

$$k(T) = \sum_{j=0}\frac{k_j(T)}{Q_{rot}}(2j+1)e^{-Bj(j+1)hc/k_BT} \quad (2.13)$$

where B [this should not be confused with B_J in eq 2.11] is the rotational constant of H_2, h is Planck's constant, c is the velocity of light in a vacuum, and Q_{rot} is the rotational partition function that assumes the general form

$$Q_{rot} = \sum_{j=0}(2j+1)e^{-Bj(j+1)hc/k_BT} \quad (2.14)$$

with the summations in eqs 2.13 and 2.14 extending to all rotational states ($j \le 5$) necessary for convergence.

3. Results and Discussion

Figure 1 shows the calculated reaction probabilities as a function of the collision energy for H_2 set initially in its ground rovibrational state. Except for $J = 0$, in the considered energy range of 0.01−1.0 eV, all reaction probabilities show an abrupt rise near threshold and a tendency to flatten with increasing collision energy. In the case of $J = 0$, the reaction probability tends to decline with increasing collision energy after a plateau between 0.1 and 0.5 eV. The resonance structures observed in the quantum reaction probabilities can be explained from the deep potential energy well on the $1\,^2A''$ surface. However, such a resonance structure is somewhat attenuated in the CC results, as revealed by the comparison between the CC and CS probabilities for $J = 10$ and 15 in Figure 2. Indeed, despite some quantitative differences concerning the resonance structures and the apparent tendency of the CC curve to lie on average above the CS one, there is generally good qualitative agreement between the probabilities calculated from those two methods. It seems then safe to conclude that the cheaper CS approximation performs well for the title reaction.

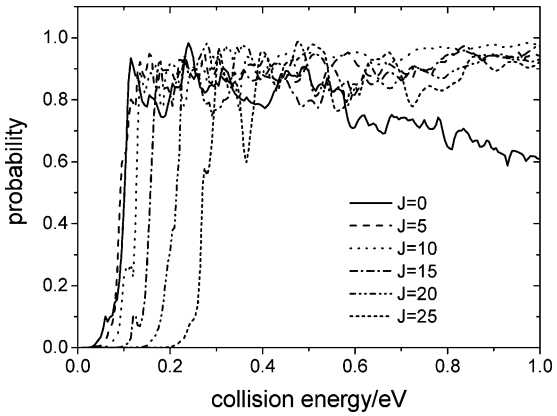

Figure 1. The CS calculated reaction probabilities as a function of collision energy ranging from 0.01 to 1.0 eV for H_2 initially in its ground rovibrational state, and for total angular momentum $J = 0$ (solid line), $J = 5$ (dashed line), $J = 10$ (dotted line), $J = 15$ (dash−dot line), $J = 20$ (dash−dot-dot line), and $J = 25$ (short-dash line).

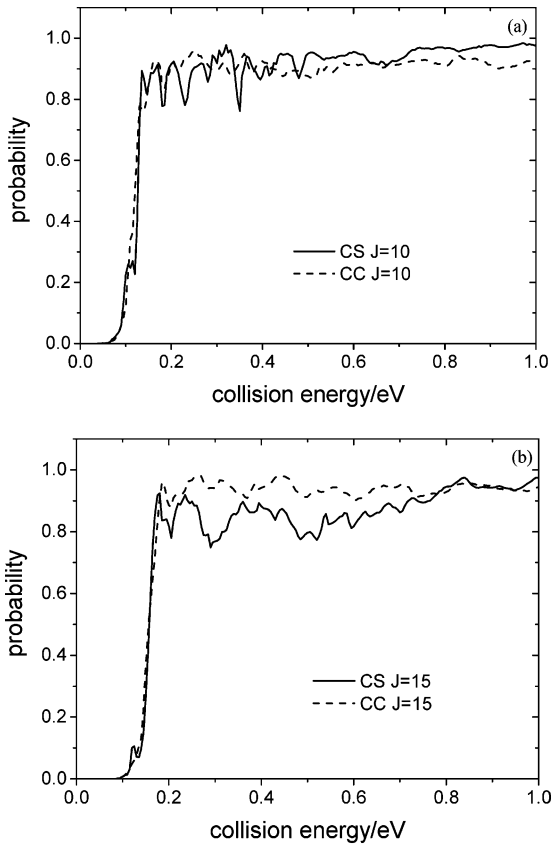

Figure 2. A comparison between the CS (solid line) and CC (dashed line) calculated reaction probabilities: (a) $J = 10$ and (b) $J = 15$. The reactant H_2 is initially in its ground rovibrational state.

Figure 3 shows the calculated total reaction cross section when H_2 is initially in its ground rovibrational state. A multiplicative factor of 1/5 has been included to account for the electronic degeneracy: there are 10 electronic doublet states in $N(^2D) + H_2$ but only 2 of those states are sampled when studying the dynamics on the $1\,^2A''$ potential energy surface. It can be seen that the cross section rises for low collision energies

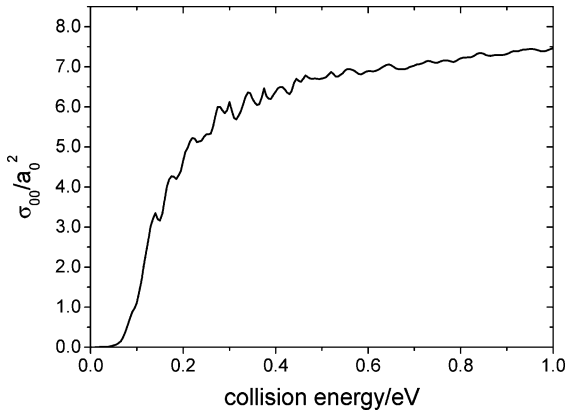

Figure 3. Calculated CS excitation function [total reactive cross section (in atomic units) as a function of collision energy] for H_2 in its ground rovibrational initial state.

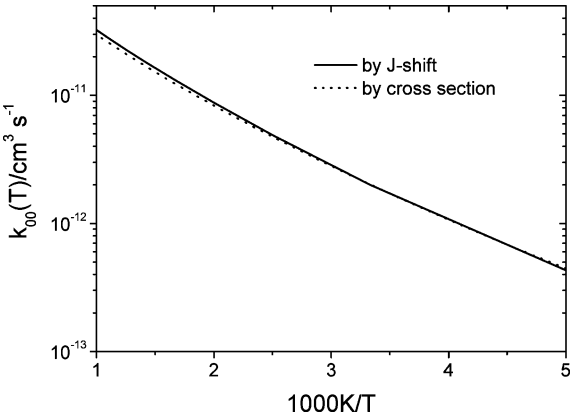

Figure 4. Rate constants for initial rotational state $j = 0$ obtained directly from cross sections (dotted line) and by using the *J*-shift techniques (in solid line).

and then flatten to reach a plateau at the highest energies studied in the present work. Some resonance peaks of the reaction probabilities are seen to survive after summing over the total angular momentum *J*, being even observed in the quantum total cross sections. Figure 4 shows the calculated rate constant for N(^{2}D) + H_2 when H_2 is initially in its ground rovibrational state. Both the results calculated from the total reaction cross section and *J*-shifting technique are given. For this comparison, we have used three values of *J* (namely 0, 10, and 30) to calibrate the *J*-shifting approach. It can be seen that despite a slight difference for high temperatures, the rate constants calculated by the two methods are almost the same particularly for low-temperature regimes. The good agreement between the results obtained from these two methods then indicates that the *J*-shifting scheme works well for the title reaction. Thus, to save computational resources, we will use only the *J*-shifting method in the calculations of the rate constant for the various initial rotational states here considered.

Figure 5a−f show the calculated reaction probabilities for $j = 1-5$ with $J = 0$, 10, and 30 (all calculations reported in this work refer to the reactant molecule being initially in its ground vibrational state, $v=0$, since this is essentially the only populated vibrational state for the range of temperatures here considered). Note that the results in panels (c) and (d) for $k = \pm 1$ should be identical with exact numerics. Clearly, the results indicate that the rotational excitation of H_2 does not have a significant influence in reactivity. In fact, only a slight difference is observed among the various *j*-state values. In Figure 6 we show the corresponding rate constants for initial rotational states of $j = 0-5$ as obtained from the *J*-shifting technique described above (i.e., based on values of J=0, 10, and 30). Such rate constants are seen to be very similar, with only a slight increase being observed for high rotational numbers. The only exception to this pattern is the rate constant for $j = 0$ which is found to be slightly larger than $j = 1$ at low temperatures. Balucani et al.[8] surmised that the differential cross section (DCS) for the initial state $j = 2$ should be very similar to the corresponding result for $j = 3$ at a collision energy of 8.8 kJ mol^{-1}. Such an assumption appears validated if judged by the present similar rate constants for $j = 2$ and 3. However, further evidence concerning the product angular distribution is necessary by performing state-to-state quantum calculations, which is beyond the scope of the present work.

The rate constants obtained by statistically averaging over the rotational states $j = 0-5$ are compared with the experimental measurements[2] in Figure 7. Such quantum numbers are sufficient to warrant accurate rate constants up to the highest temperatures here considered. All diatomic rotational states have been considered, thus leaving aside any specificities regarding the ortho-para quantum statistics of H_2. Clearly, our results are seen to be in good agreement with the reported measurements, especially having in mind that there is a missing contribution to the N(^{2}D) + H_2 reaction which refers to the reactive processes occurring on the upper sheet that forms a Renner-Teller pair with the title potential energy surface. In Figure 7, we plot also the QCT results of Pederson et al.[10] and Ho et al.[12] Clearly, the present rate constants calculated on the DMBE surface compare very well with the experimental results. They are also seen to be only slightly smaller than the QCT rate constants of Ho et al.[12] on their new potential energy surface, which has barrier heights for H-abstraction and insertion that are about 0.3 kcal mol^{-1} smaller than in the DMBE potential energy surface. It is also seen that both the QCT rate constants calculated on a single 1 ^{2}A″ surface (ground-state, GS) and the two Renner-Teller surfaces 1 ^{2}A″ and 1 ^{2}A′ (excited-state, ES) are somewhat smaller than the present quantum results. Since the three theoretical calculations employed different potential energy surfaces, it will be necessary to take into account the differences on such potential energy surfaces to make the comparison more reasonable. The C_{2v} barrier of the DMBE surface is 2.16 kcal mol^{-1} as predicted from the DMBE-SEC corrected MRCI/aug-cc-pVQZ calculations. However, its value is 1.93 kcal mol^{-1} (with the Davidson correction, DC) or 2.29 kcal mol^{-1} (without DC) on the surface of Pederson et al.[10] and 1.80 kcal mol^{-1} on the new potential energy surface of Ho et al.[12] Note that both such surfaces have been modeled using less accurate MRCI/aug-pVTZ calculations (see ref 20 for further comparisons). Thus, the larger rate constants (in closer agreement with experiment) obtained in the QCT calculations of Ho et al.[12] may partly be due to the lower C_{2v} insertion barrier of their potential energy surface. We emphasize that the DMBE[20] potential energy surface predicts a C_{2v} barrier height somewhat larger than the surface of Ho et al.,[12] while being based on higher level ab initio calculations than the latter. Thus, the fairly good agreement between the experimental data and the present quantum results demonstrates the high accuracy of the DMBE potential energy surface also in dynamics calculations. Moreover, since the DMBE surface has a C_{2v} barrier which is closer to that of the Pederson et al.'s surface,[10] the comparison with their results suggests that the larger rate constants obtained from the present quantum calculations may partly be due to tunneling effects. Finally, the good agreement achieved in the comparison between the measured rate constants and the present quantum calculations

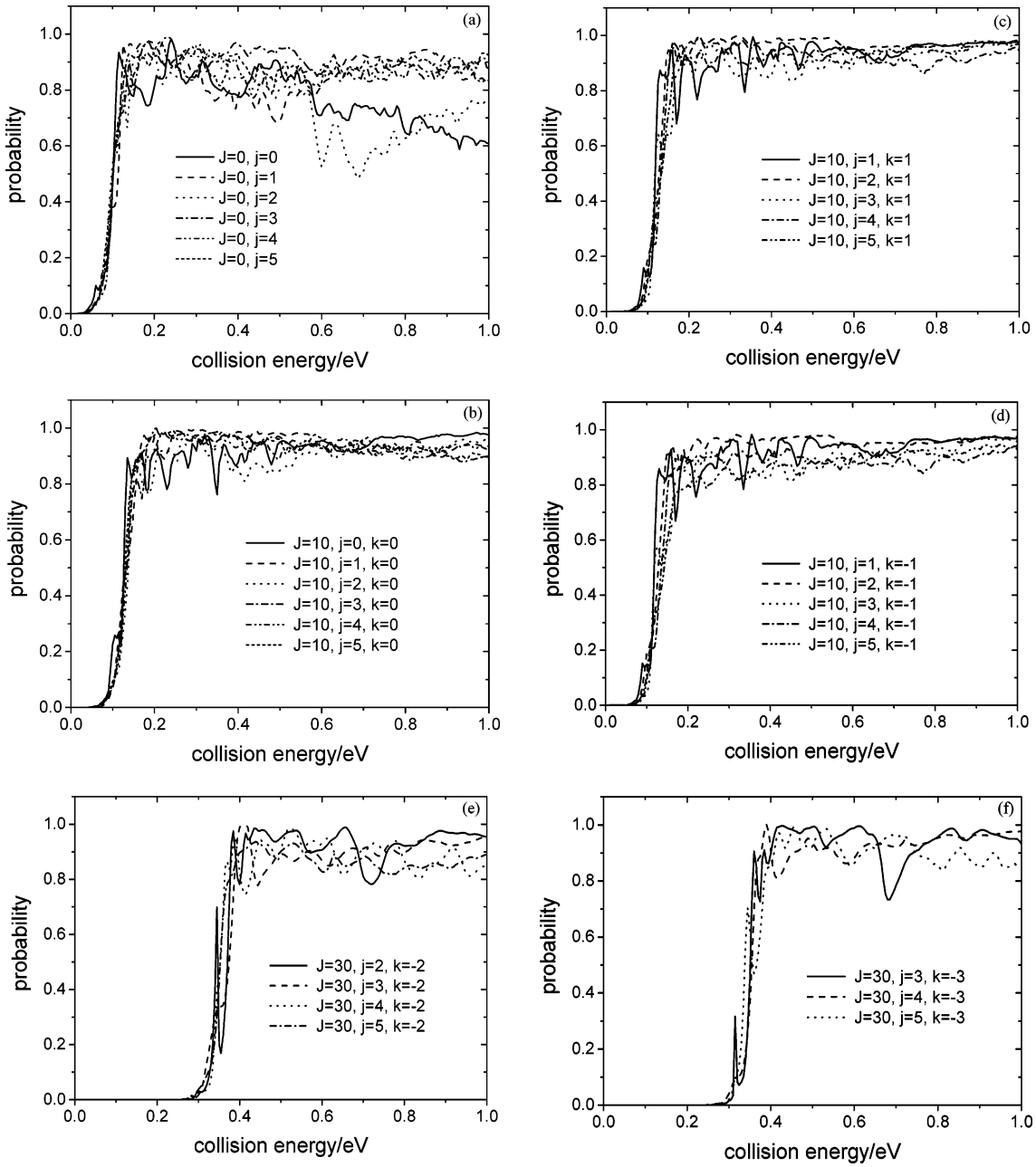

Figure 5. CS probabilities for initial rotational states $j = 0-5$ and $J = 0$, 10, and 30.

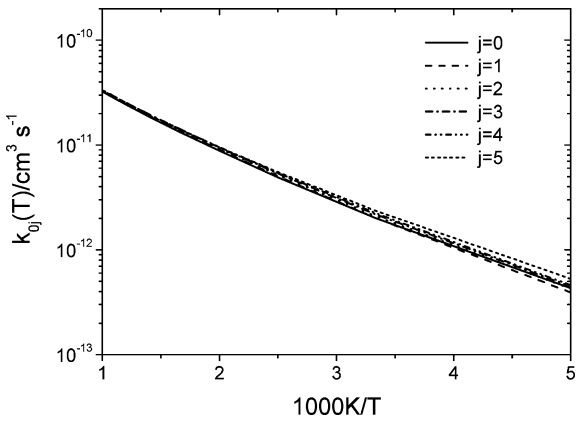

Figure 6. Rotationally specific rate constants calculated by using the *J*-shifting technique for initial rotational states $j = 0$ (solid line), $j = 1$ (dashed line), $j = 2$ (dotted line), $j = 3$ (dash−dot line), $j = 4$ (dash−dot-dot line), and $j = 5$ (short-dash line).

(which were performed only on the ground state adiabatic potential energy surface) suggests that nonadiabatic effects have only a minor contribution to the rate constant, in agreement with what has been found in the nonadiabatic studies of Schatz and co-workers[10,11] which employed the surfaces for the $1\ ^2A''$ and $1\ ^2A'$ electronic states of NH_2. Of course, information on the rotational and vibrational distributions of the products would be valuable to further assess the present reaction and test the accuracy of the DMBE potential energy surface. Although this information cannot be reported here due to not having performed state-to-state time-dependent wave packet calculations thus far, we hope that such an analysis will be addressed in future work.

4. Conclusions

We have performed quantum scattering calculations on the recently reported DMBE potential energy surface for $NH_2(1^2A'')$ to calculate reaction probabilities, total reaction cross sections, and rate constants for the title reaction. Both the CS reaction-probabilities for the rotational states $j = 0-5$ and CS total

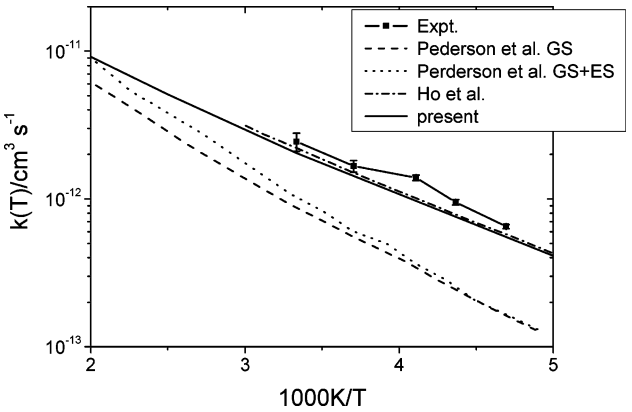

Figure 7. Comparison of the rate constant statistically averaged over a Boltzmann distribution of rotational states with the experimental measurements and other theoretical (QCT) results: solid line, this work; solid line with solid squares, experiment;[2] dashed and dotted lines, QCT results of Pederson et al.;[10] dash−dot line, QCT calculation of Ho et al.[12]

reaction cross section for $j = 0$ have shown resonance structures, with a general tendency to increase with collision energy over the energy range of 0.01−1.0 eV. A comparison between the CS and CC probabilities suggests that the Coriolis coupling may play a small role in an accurate quantum calculation, thus validating the cheaper CS calculations here reported for the title system. The calculated rate constants for $v = 0, j = 0$ obtained by using the *J*-shifting approach have also been shown to be in good agreement with those determined from the total cross sections, thus suggesting that such an approach may produce fairly reliable results for the title system. Based on this observation, we have reported rate constants for $v = 0, j = 1-5$ by using the *J*-shifting technique. Statistically rotationally averaged rate constants have also been calculated and found to be in good agreement with existing experimental measurements. Our results have also been found to agree strikingly well with QCT results based on a potential energy surface with a somewhat lower C_{2v} barrier height. Such an agreement may partially be due to a compensation of barrier height and tunneling effects that are neglected on the trajectory results. Quasiclassical trajectory calculations as well as more rigorous CC quantum results on the present DMBE potential energy surface would then be valuable to clarify such issues. This as well as studies involving other relevant electronic states of NH_2 are currently under way and will be reported elsewhere.

Acknowledgment. This work has the support of NKBRSF (1999075302), the Knowledge Innovation Program of the Chinese Academy of Sciences (INF105-SCE-02-08) and NSFC (20373071, 20333050), and Fundação para a Ciência e a Tecnologia, Portugal (POCTI/40154/QUI/2001). This work was also supported in part by the European Community's Human Potential Program under contract HPRN-CT-2002-00170.

References and Notes

(1) Dodd, J. A.; Lipson, S. J.; Flanagan, D. J.; Blumberg, W. A. M.; Person, J. C.; Green, B. D. *J. Chem. Phys.* **1991**, *94*, 4301.
(2) Suzuki, T.; Shihira, Y.; Sato, T.; Umemoto, H.; Tsunashima S. J. *J. Chem. Soc., Faraday Trans.* **1993**, *89*, 995.
(3) Kobayashi, H.; Takayanagi, T.; Yokoyama, K.; Sato, T.; Tsunashima, S. J. *J. Chem. Soc., Faraday Trans.* **1995**, *91*, 3771.
(4) Pederson, L. A.; Schatz, G. C.; Ho, T.-S.; Hollebeek, T.; Rabitz, H.; Harding, L. B.; Lendvay, G. *J. Chem. Phys.* **1999**, *110*, 9091.
(5) Umemoto, H.; Matsumoto, K. *J. Chem. Phys.* **1996**, *104*, 9640.
(6) Umemoto, H.; Asai, T.; Kimura, K. *J. Chem. Phys.* **1997**, *106*, 4985.
(7) Honvault, P.; Launay, J. *J. Chem. Phys.* **1999**, *111*, 6665.
(8) Balucani, N.; Cartechini, L.; Capozza, G.; Segoloni, E.; Casavecchia, P.; Volpi, G. G.; Aoiz, F. J.; Bañares, L.; Honvault, P.; Launay, J. *Phys. Rev. Lett.* **2002**, *89*, 013201.
(9) Alagia, M.; Balucani, N.; Cartechini, L.; Casavecchia, P.; Volpi, G. G.; Pederson, L. A.; Schatz, G. C.; Lendvay, G.; Harding, L. B.; Hollebeek, T.; Ho, T.-S.; Rabitz, H. *J. Chem. Phys.* **1999**, *110*, 8857.
(10) Pederson, L. A.; Schatz, G. C.; Hollebeek, T.; Ho, T.-S.; Rabitz, H.; Harding, L. B. *J. Phys. Chem. A* **2000**, *104*, 2301.
(11) Santoro, F.; Petrongolo, C.; Schatz, G. C. *J. Phys. Chem. A* **2002**, *106*, 8276.
(12) Ho, T.-S.; Rabitz, H.; Aoiz, F. J.; Bañares, L.; Vázquez, S. A.; Harding, L. B. *J. Chem. Phys.* **2003**, *119*, 3063.
(13) Qu, Z.-W.; Zhu, H.; Schinke, R.; Adam, L.; Hack, W. *J. Chem. Phys.* **2005**, *122*, 204313.
(14) Kobayashi, H.; Takayanagi, T.; Tsunashima, S. *Chem. Phys. Lett.* **1997**, *277*, 20.
(15) Umemoto, H.; Terada, N.; Tanaka, K. *J. Chem. Phys.* **2000**, *112*, 5762.
(16) Gray, S. K.; Balint-Kurti, G. G.; Schatz, G. C.; Kin, J. J.; Liu, X.; Harich, S.; Yang, X. *J. Chem.* Phys. **2000**, *113*, 7330.
(17) Takayanagi, T. *J. Chem. Phys.* **2002**, *116*, 2439.
(18) Gray, S. K.; Goldfield, T. M.; Schatz, G. C.; Balint-Kurti, G. G. *Phys. Chem. Chem. Phys.* **1999**, *1*, 1141.
(19) Aoiz, F. J.; Bañares, L.; Castillo, J. F.; Brouard, M.; Denzer, W.; Vallance, C.; Honvault, P.; Launay, J. M.; Dobbyn, A.; Knowles, P. J. *Phys. Rev. Lett.* **2001**, *86*, 1729.
(20) Varandas, A. J. C.; Poveda, L. A. *Theor. Chem. Acc.* In press.
(21) Varandas, A. J. C. *J. Chem. Phys.* **1989**, *90*, 4379.
(22) Zhang, J. Z. H.; Dai, J.; Zhu, W. *J. Phys. Chem. A* **1997**, *101*, 2746.
(23) Zhang, D. H.; Zhang, J. Z. H. *J. Chem. Phys.* **1994**, *101*, 1146.
(24) Fleck, J. A., Jr.; Morris, J. R.; Feit, M. D. *Appl. Phys.* **1976**, *10*, 129.
(25) Nussbaumcr, H. J. *Fast Fourier Transform and Convolution Algorithms*, 2nd ed.; Springer-Verlag, Berlin, 1982.
(26) Light, J. C.; Hamilton, I. P.; Lill, J. V. *J. Chem. Phys.* **1985**, *82*, 1400.
(27) Aoiz, F. J.; Bañares, L.; Castillo, J. F. *J. Chem. Phys.* **1999**, *111*, 4013.
(28) Mielke, S. L.; Lynch, G. C.; Truhlar D. G.; Schwenke D. W. *J. Phys. Chem.* **1994**, *98*, 8000.
(29) Zhang, D. H.; Zhang, J. Z. H. *J. Chem. Phys.* **1999**, *110*, 7622.